Journal of Optoelectronics and Advanced Materials Vol. 3, No. 2, June 2001, p. 287 - 294

ON THE CHANGES IN THE STRUCTURAL AND OPTICAL PROPERTIES ACCOMPANYING THE ATHERMAL PHOTOVITRIFICATION PHENOMENON IN $As_{50}Se_{50}$ THIN FILMS

R. Prieto-Alcón, J. M. González-Leal, R. Jiménez-Garay, E. Márquez

Departamento de Física de la Materia Condensada. Facultad de Ciencias
Universidad de Cádiz. 11510 – Puerto Real (Cádiz) Spain

The effect of successive annealing-illumination cycles on the structural and optical properties of wedge-shaped $As_{50}Se_{50}$ amorphous chalcogenide thin films, has been studied. It is observed that illumination increases the thickness and shrinks the bandgap. Annealing of the chalcogenide films, before or after illumination, decreases the thickness. However, although annealing after illumination increases the bandgap, when this treatment is carried out upon the as-evaporated films, the bandgap decreases. The photostructural changes have been explained in terms of two different mechanisms, which can coexist. One of them involving the repulsion and slip motion of the 2D structural layers comprising the 'pyramidal' network, as a consequence of the negative charging of these structural layers, by electron accumulation in conduction-band tails, and the other, involving the As_4Se_4 molecules, typical of thermally-evaporated As-rich chalcogenides films, and forming particularly the crystalline form of medium-thickness (1÷2 μm) $As_{50}Se_{50}$ films.

(Received June 4, 2001; accepted June 11, 2001)

Keywords: Amorphous chalcogenides, Thin films, Structural and optical properties, Athermal photovitrification

1. Introduction

Amorphous chalcogenides exhibit a wide variety of photoinduced structural transformations [1]. A flexible structure due to the presence of lone-pair electrons, on the one hand, and localization of carriers because of the disorder, on the other hand, are both responsible for this light-induced structure-related metastability. As a consequence of such photoinduced changes, optical absorption and many other properties of these amorphous materials including refractive index, density, elastic constants, photoconductivity and chemical solubility, are altered drastically.

Let us consider a process for producing amorphous state, namely the athermal light-induced vitrification of crystalline $As_{50}Se_{50}$ thin films. The essence of this process is as follows: Amorphous $As_{50}Se_{50}$ films deposited onto either glass or silicon wafer substrates can crystallize by thermal annealing, and subsequent irradiation will cause the vitrification of the films. It has been shown that these amorphous films, when evaporated onto glass substrates, crystallized into different structures, depending on the annealing temperature [2]. On the other hand, the photovitrification phenomenon depends on the film thickness [2], which underlines the influence of the interaction between the film and the substrate. In fact, we have analyzed in a previous work [3], the role played by the silicon substrate in this particular light-induced process. The photoamorphization, which is also dependent on the spectral irradiance of the light source employed [3], is reversible and we will study the results corresponding to the first two crystallization-amorphization cycles. In the present work we will focus our attention on the changes in the structural and optical properties, which accompany the athermal photovitrification phenomenon in $As_{50}Se_{50}$ thin films.

2. Experimental details

The bulk starting material was prepared by direct synthesis from 5N purity elements, heated together in an evacuated quartz ampoule at a temperature of 950 ºC, for about 24 h. After the synthesis, the melt was air-quenched, resulting in a bulk glass of the required chemical composition. X-ray diffraction measurements (Philips, model PW 1710), using Cu Kα radiation (1.54 Å), proved that the ingot was amorphous. The studied amorphous thin films were prepared by thermal evaporation of the $As_{50}Se_{50}$ bulk glass onto room-temperature glass substrates, in a vacuum of $\approx 10^{-6}$ Torr, using for this purpose a conventional coating unit (Edwards, model E306A). During evaporation, the substrates were rotated (45 rpm) in order to improve the degree of film thickness uniformity, and the deposition rate was ≈ 1 nm s^{-1}, this quantity having been continuously measured by a quartz-crystal monitor (Edwards, model FTM-5). Electron microprobe analysis of the as-deposited $As_{50}Se_{50}$ thin films showed that the film stoichiometry is correct to ± 0.5 at.%. The samples were annealed at 150 ºC (T_g = 164 ºC) for periods of time of, typically, 72 h in a $\approx 10^{-3}$ Torr vacuum. Illumination of the glass films was carried out using a 500 W high-pressure mercury lamp (Oriel, model 6285), through an IR-cut filter, providing broadband white light (with a very high UV output), using a light intensity of ≈ 50 mW cm^{-2}. X-ray diffraction analysis was also used in order to examine the glassy or crystalline nature of the films.

The optical transmission spectra used in this study were obtained over the 300÷2000 nm spectral region by a double-beam UV/Vis/NIR spectrophotometer (Perkin-Elmer, model Lambda-19). The spectrophotometer was set with a slit width of 1 nm. It was therefore unnecessary to make slit width corrections, since that value of the slit width was much smaller than the different linewidths. The area of illumination, over which a single optical transmission spectrum was obtained, was approximately 1 mm × 10 mm. A surface-profiling stylus (Sloan, model Dektak 3030) was used to determine the thickness of the films, for the sake of comparison with the results derived from the optical transmission spectra. Typical thicknesses of the as-deposited films studied were around 1 μm, and, thus, according to Kolobov and Elliott [2], our samples can be considered as medium-thickness (1÷2 μm) films.

Table 1. Values of the average thickness, $\bar{d}$, thickness variation, Δd, dispersion parameters, E_o and E_d (single-oscillator analysis), and optical bandgap, E_g^{opt} (Tauc's extrapolation), for the $As_{50}Se_{50}$ chalcogenide thin films under study.

State	$\bar{d}$ (nm)	Δd (nm)	E_o (eV)	E_d (eV)	E_g^{opt} (eV)
As-evaporated	1119 ± 10 (0.9 %)	18 ± 1	4.07 ± 0.02	24.08 ± 0.1	1.87 ± 0.01
First annealing	1066 ± 11 (1.1 %)	28 ± 1	3.92 ± 0.03	25.86 ± 0.2	1.81 ± 0.01
First illumination	1109 ± 19 (1.7 %)	34 ± 2	3.64 ± 0.03	19.56 ± 0.2	1.78 ± 0.01
Second annealing	930 ± 35 (3.8 %)	—	3.83 ± 0.04	24.68 ± 0.2	1.81 ± 0.02
Second illumination	1030 ± 39 (3.8 %)	—	3.68 ± 0.04	20.59 ± 0.3	1.73 ± 0.02

3. Results and discussion

The athermal photovitrification phenomenon in $As_{50}Se_{50}$ films, has been studied from the optical point of view by means of two different methods, enabling the determination of the average thickness and the refractive index of the as-deposited, annealed and exposed $As_{50}Se_{50}$ non-uniform films (see Table 1). The first one, which is based on creating the upper and lower envelope curves of the optical transmission spectrum, at normal incidence, assumes the film thickness, d, to vary linearly

over the illuminated area, i.e., $d = \overline{d} + \eta\Delta d$, where $-1 \le \eta \le 1$. Δd refers to the variation in thickness from the average thickness $\overline{d}$, as shown in Fig. 1. The applicability of this method is limited by the condition, $0 < \Delta d < \lambda/4n$. Details about this first optical characterization procedure can be found in [4-6].

Due to the larger degree of morphological alteration shown by the $As_{50}Se_{50}$ thin films submitted to a second annealing-illumination cycle, the above-mentioned condition is no longer satisfied. Therefore, a second optical characterization method, based only on wavelengths measurements, was used to determine the average thickness and the refractive index of the samples. Such a procedure takes into consideration the shift of the transmission spectrum at oblique (30º) incidence towards shorter wavelengths, with respect to the transmission spectrum taken at normal incidence. For details of this second characterization procedure see our previous works [7,8].

Fig. 1 shows the optical transmission spectra at normal incidence, in the short-wavelength region, for the as-deposited, crystallized and photoamorphized $As_{50}Se_{50}$ thin films, corresponding to

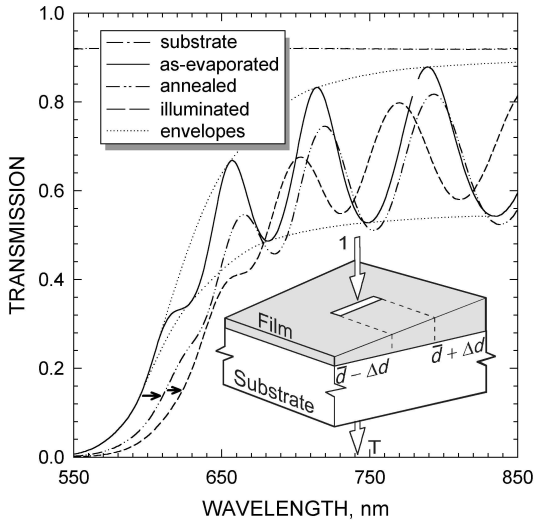

Fig. 1. Typical optical transmission spectra, in the short-wavelength region, for the as-evaporated, annealed (crystallized) and illuminated (photovitrified) $As_{50}Se_{50}$ thin layers. The envelopes corresponding to the as-evaporated layer are also drawn as a representative example. Additionally, a diagram representing a weakly-absorbing thin layer, with a linear variation in thickness on a thick transparent substrate, is also displayed.

the first annealing-illumination cycle. An irreversible shift of the optical transmission spectrum towards longer wavelengths is observed in the interference-free region of this transmission spectrum when the as-evaporated film is annealed (i.e., thermal darkening). Subsequent illumination of the film induces again a shift of the optical transmission spectrum towards longer wavelengths (i.e., photodarkening), but it is reversible, in the sense that post-illumination annealing returns partly the interference-free region to its initial annealed state.

It has been found that the refractive index increases with annealing and decreases upon illumination, under the initial value (see Fig. 2). The spectral dependence of the refractive index has been fitted to the Wemple-DiDomenico single-oscillator model [10]:

$$\varepsilon_1(\hbar\omega) = n(\hbar\omega)^2 = 1 + \frac{E_o E_d}{E_o^2 - (\hbar\omega)^2} \tag{1}$$

where E_o is the single-oscillator energy (typically near the main peak of the $\varepsilon_2(\hbar\omega)$-spectrum) and E_d is the dispersion energy. By plotting $(n^2 - 1)^{-1}$ against $(\hbar\omega)^2$ and fitting a straight line, as shown in the

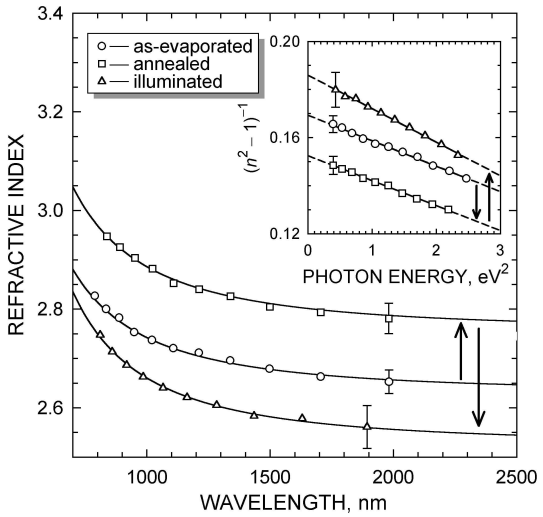

Fig. 2. Refractive index versus wavelength. Also, it is shown in the inset, a plot of the refractive-index factor $(n^2 - 1)^{-1}$ versus $(\hbar\omega)^2$, for the as - evaporated, crystallized and photoamorphized layers.

inset of Fig. 2, E_o and E_d are determined directly from the slope, $(E_oE_d)^{-1}$, and the intercept, E_o/E_d, on the vertical axis. The values of the dispersion parameters for the as-evaporated, crystallized and photovitrified films are listed in Table 1 (two annealing-illumination cycles). The trend of E_o is such that it is verified that $E_o \approx 2\times E_g^{opt}$, E_g^{opt} being the so-called Tauc gap, which is a widely accepted measure of the bandgap and will be formally introduced below, whereas E_d obeys the following empirical relationship [10,11]:

$$E_d = \beta\, N_c\, Z_a\, N_e \quad \text{(eV)} \tag{2}$$

where N_c is the coordination number of the cation nearest-neighbour to the anion, Z_a is the formal chemical valency of the anion, N_e is the effective number of valence electrons per anion and $\beta = 0.37 \pm 0.04$ eV, for covalent crystalline and amorphous materials.

In addition, the following relationship was proposed by Wemple [11]:

$$E_d^a / E_d^x = (\rho^a / \rho^x)(N_c^a / N_c^x \tag{3}$$

where ρ represents the mass density (the film thickness could be used instead, because changes in the mass of the films were not measured), and 'a' and 'x' refer to the amorphous and crystalline forms, respectively. The thermal densification process, as well as the photoinduced volume expansion, which have been observed, respectively, upon annealing of the as-deposited $As_{50}Se_{50}$ film, and illumination of the crystallized film (see the thicknesses listed in Table 1), have to be considered to explain the variation of the oscillator strength. Although this analysis is also qualitatively valid for the second annealing-illumination cycle, we will point our discussion to the first annealing-illumination cycle. An increase of ≈ 7 % is observed in the E_d-value as a consequence of the annealing process. By means of Eq. (3), we find that the difference between N_c's, before and after annealing, is less than 2 %; therefore, the small change in N_c indicates a rather insignificant change in the average coordination number in the short-range region. Moreover, E_d calculated from Eq. (2) (considering $N_c = 3$, $Z_a = 2$, $N_e = (50 \times 5 + 50 \times 6)/50 = 11$ [11]) was found to be 24.42 ± 2.6 eV; that is, allowing the corresponding scatter in β, E_d is certainly close to the experimental values of the as-deposited and annealed films. Going one step further, the comparison of the E_d-values corresponding to the annealed and illuminated films shows a large decrease of ≈ 24 %, accompanied by a decrease of the mass density of

≈ 4 %. The extra 20 % reduction in the E_d-value, as a consequence of the photovitrification of the crystallized film, could be due to a decrease in the effective As coordination number.

On the other hand, following Swanepoel's ideas [4,12], in the strong-absorption region, the values of the optical absorption coefficient, α, have been directly derived from the transmittance measurements, using Eq. (22) from [12]. Fig. 3 shows the optical absorption spectra, $\alpha(\hbar\omega)$, for the as-deposited, crystallized and photoamorphized $As_{50}Se_{50}$ films. It can be seen a shift of the absorption edge to lower photon energies as a consequence of the annealing, as well as the illumination treatment. According to Tauc [13], the spectral dependence of the absorption coefficient in the strong-absorption region ($\alpha \tau 10^4$ cm^{-1}), is given by the following quadratic equation:

$$\alpha(\hbar\omega) = B\,\frac{(\hbar\omega - E_g^{opt})^2}{\hbar\omega} \tag{4}$$

where B is an energy-independent constant. Formally, the Tauc gap, E_g^{opt}, is obtained as the intercept of the plot of $(\alpha\hbar\omega)^{1/2}$ against $\hbar\omega$. This graph is shown in the inset of Fig. 3 for the as-evaporated, annealed and illuminated $As_{50}Se_{50}$ films. The values of E_g^{opt}, thus determined, lead us to the conclusion that a clear reversible photodarkening process accompanies the present photoinduced phenomenon.

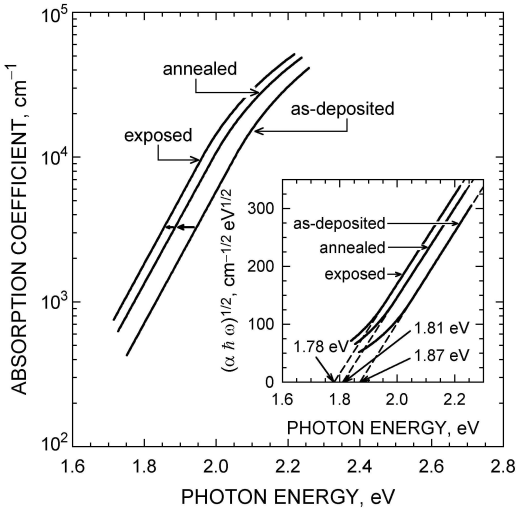

Fig. 3. Optical absorption spectra for the as-deposited, annealed and exposed $As_{50}Se_{50}$ films. In the inset, the determination of the optical bandgap based on the Tauc law.

The relative changes in the average thickness and in the Tauc gap, after two annealing-illumination cycles, are displayed in Fig. 4. These results clearly indicate that, illumination always expands the films and decreases E_g^{opt}, while annealing, before or after illumination, is found to contract the $As_{50}Se_{50}$ films. However, although annealing after illumination increases the bandgap, when the thermal treatment is carried out upon the as-evaporated films, the bandgap decreases, instead. These results suggest a certain correlation between these two types of changes.

We have observed 'giant' changes in $\overline{d}$ and E_g^{opt}. Increases in the average thickness of up to ≈ 4 %, in the case of the illumination after the first annealing, and of up to ≈ 11 %, in the case of the illumination after the second annealing, have been found. In which the bandgap is concerned, a decrease larger than 4 % has been obtained with the illumination after the second annealing. Other authors [14-18] have also observed large changes in the thickness and the optical bandgap of As-based and Ge-based obliquely-deposited chalcogenide thin films. Furthermore, it was found in [18]

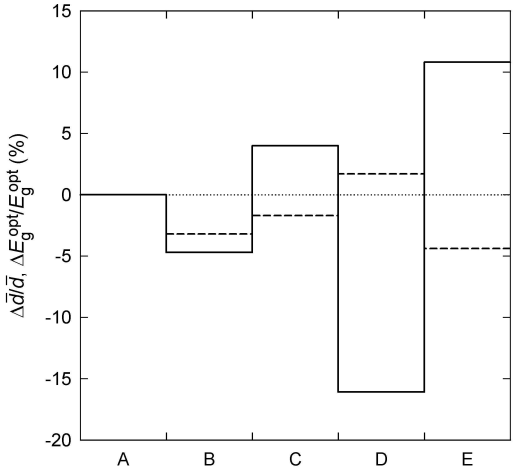

Fig. 4. Variation in relative changes in the average thickness $\bar{d}$ (solid line), and Tauc gap E_g^{opt} (dashed line), of the $As_{50}Se_{50}$ thin layers. Measurement conditions are represented by: A, as-evaporated; B, first annealing; C, first illumination; D, second annealing; E, second illumination.

that post-illumination annealing causes the changes to revert to nearly the initial conditions. However, the morphological changes undergone by our wedge-shaped $As_{50}Se_{50}$ chalcogenide films, because the successive thermal and optical treatments, make somehow the results obtained by means of the two different optical characterization methods, to be only comparable up to a certain degree.

It is believed that a change in the interaction of chalcogen lone-pair electrons is responsible for the photodarkening phenomenon. The increase in lone-pair–lone-pair interactions causes a broadening of the valence band, giving rise to a reduction in the optical bandgap. Various models have been proposed to explain this mechanism [19-21]. In particular, the expansion and slip motion model was proposed by Shimikawa *et al*. [19] to explain the photoinduced changes in volume observed in normally-deposited films. Recently, Kuzukawa *et al*. [17] have justified the 'giant' changes observed in the thickness and the bandgap of As_2Se_3 and As_2S_3 thin films, as a consequence of illumination, on the basis of the same model. The essence of this model is schematically illustrated in Fig. 5 and it can be summarized as follows: It is assumed that amorphous chalcogenides contain disordered structural layers as a constituent element of their structure, and considered that during illumination there is an accumulation of electrons in these layered clusters, which causes Coulomb repulsion between them and therefore it gives rise to volume expansion. Unlike these electrons, which reside in the conduction-band tails, photocreated holes diffuse away to a non-illuminated area through the valence band or their tail states. Since it has been shown that the rate of volume expansion is greater than photodarkening [22], it is expected that photodarkening is not induced at this stage. Instead, it is believed that in conjunction with the occurrence of the interaction between adjacent clusters, a slip motion along the structural layer is generated, which causes an increase in the energy of the highest occupied states in the valence band, due to an increase in the lone-pair–lone-pair interactions. Thus, although the conduction band remains practically unchanged, the valence band gets wider [23].

On the other hand, since thermally-evaporated arsenic-rich amorphous films, such as $As_{50}Se_{50}$, can be regarded as a mixture of As_2Se_3 and As_4Se_4 molecules, whose structure can be represented as As_4Se_4 molecules dissolved in a matrix formed by $AsSe_3$ pyramids, it could be suggested that two mechanisms could coexist. One of them would involve the 'pyramidal' network (repulsion and slip motion of the structural layers), whereas the other would deal with As_4Se_4 molecules. These molecules have a cage-like structure, in which a square of Se atoms bisects a distorted tetrahedron of As atoms. The average As-As bond length in As_4Se_4 is 2.57 Å, and the As-As-Se bond angle subtended at either one of the As atoms comprising the As-As bonds, is 101.2º.

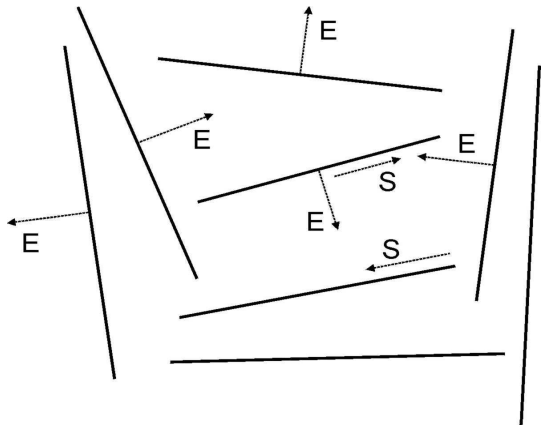

Fig. 5. Schematic illustration of the layered clusters in amorphous chalcogenides.
The expansion and slip motions are indicated by arrows E and S, respectively.

If one compare those values with the corresponding bond distance and bond angle in *a*-As, 2.49 Å and 98º, respectively, it is found that they are larger in the case of the As_4Se_4 molecule. The intermolecular distances, less than 3.70 Å, are shorter than the predicted van der Waals distance of 4.0 Å, which could be associated with relatively strong intermolecular interactions. As-As bonds play an important, although not predominant, role in reversible photodarkening in well-annealed As-rich thin-film samples [24]. An increase in the As-As bond concentration, as a consequence of illumination, leads to a decrease of the bandgap, owing to formation of electronic states associated with such bonds at the top of the valence band. Similarly, the subsequent annealing of the sample will lead to a decrease in the As-As bond concentration. Therefore, the bandgap will increase because breaking of As-As bonds will replace the electronic states in the gap, associated with these homopolar bonds, by non-bonding As states located near the conduction band edge.

4. Conclusions

We have studied the changes in the structural and optical properties, which take place in $As_{50}Se_{50}$ amorphous thin films, as a consequence of two successive annealing-illumination cycles. It was found that on annealing the film thickness decreases (i.e., thermal contraction), and the bandgap also decreases (i.e, thermal darkening). On subsequent illumination of the crystallized films, the thickness is found to increase (i.e., volume expansion), while the bandgap decreases (i.e., photodarkening). Post-illumination annealing decreases notably the thickness and, at the same time, increases the bandgap. Finally, the second illumination treatment gives rise to an increase of the film thickness accompanied, as before, by a decrease in the optical bandgap. We have observed 'giant' changes in both thickness and bandgap with illumination, especially after the second illumination treatment. It has also been found that the conditions of the samples after both annealing-illumination cycles, are not close to the initial conditions, although the morphological changes undergone by the wedge-shaped $As_{50}Se_{50}$ films, prevented us from obtaining results which could be easily compared.

It is suggested that in order to be able to explain all these changes, it is necessary to consider two different mechanisms. The first one would involve the expansion and slip motion of the structural layers comprising the 'pyramidal' network, and the second one operative with the As_4Se_4 molecules, typical of thermally-evaporated As-rich chalcogenides films, and forming particularly the crystalline form of medium-thickness (1÷2 μm) $As_{50}Se_{50}$ films.

Acknowledgements

This work has been supported by the CICYT (Spain), under the MAT98-0791 project.

References

[1] A. V. Kolobov, Ka. Tanaka, J. Opt. Adv. Mater., **4**, 3 (1999).
[2] A. V. Kolobov, S. R. Elliott, Philos. Mag. B, **71**, 1 (1995).
[3] R. Prieto-Alcón, E. Márquez, J. M. González-Leal, J. Opt. Adv. Mater., **2**, 139 (2000).
[4] R. Swanepoel, J. Phys. E: Sci. Instrum., **17**, 896 (1984).
[5] E. Márquez, J. B. Ramírez-Malo, P. Villares, R. Jiménez-Garay, R. Swanepoel, Thin Solid Films, **254**, 83 (1995).
[6] E. Márquez, J. M. González, R. Jiménez-Garay, S. R. Lukic, D. M. Petrovic, J. Phys. D: Appl. Phys., **30**, 690 (1997).
[7] C. Corrales, J. B. Ramírez-Malo, J. Fernández-Peña, P. Villares, R. Swanepoel, E. Márquez, Appl. Opt., **34**, 7907 (1995).
[8] C. Corrales, J. B. Ramírez-Malo, E. Márquez, R. Jiménez-Garay, Mat. Sci. Eng. B–Solid, **47** 119 (1997).
[9] S. R. Elliott, J. Non-Cryst. Solids, **81**, 71 (1986).
[10] S. H. Wemple, W. DiDomenico, Phys. Rev. B, **3**, 1338 (1971).
[11] S. H. Wemple, Phys. Rev. B, **7**, 3767 (1973).
[12] R. Swanepoel, J. Phys. E: Sci. Instrum., **16**, 1214 (1983).
[13] J. Tauc, J. Non-Cryst. Solids, **8**, 569 (1972).
[14] B. Singh, S. Rajagopalan, P. K. Bhat, D. K. Pandaya, K. L. Chopra, Solid State Commum., **29** 167 (1979).
[15] S. Rajagopalan, K. S. Harshvardhan, K. S. Malhotra, K. L. Chopra, J. Non-Cryst. Solids**, 50** 29 (1982).
[16] C. A. Spence, S. R. Elliott, Phys. Rev. B, **39**, 5452 (1989).
[17] Y. Kuzukawa, A. Ganjoo, K. Shimikawa, J. Non-Cryst. Solids**, 227**, 715 (1998).
[18] Y. Kuzukawa, A. Ganjoo, K. Shimikawa, Philos. Mag. B, **79**, 249 (1999).
[19] Ka. Tanaka, J. Non-Cryst. Solids**, 35**, 1023 (1980).
[20] A. V. Kolobov, H. Oyanagi, Ka. Tanaka, Ke. Tanaka, Phys. Rev. B, **55**, 726 (1997).
[21] K. Shimakawa, N. Yoshida, A. Ganjoo, Y. Kuzukawa, J. Singh, Philos. Mag. Lett., **77**, 153 (1988).
[22] Ke. Tanaka, Phys. Rev. B, **57**, 5163 (1998).
[23] T. Watanabe, H. Kawazoe, M. Yamane, Phys. Rev. B, **38**, 5677 (1988).
[24] G. Pfeiffer, M. A. Paesler, S. C. Agarwal, J. Non-Cryst. Solids, **130**, 111 (1991).